Low-temperature fabrication of TiC nanotube arrays by molten salt electrolysis for supercapacitor application

Tongxiang Ma[1,2], Rui Tan[1], Junyu Chen[1], Yuzheng Pan[1], Meilong Hu [1], Guang Han[1], Liwen Hu[1], Zhiming Yan[3]**

1. School of Materials Science and Engineering, Chongqing University, Chongqing 400044, China.

2. Northwest Institute for Non-Ferrous Metal Research, Xian 710016, China

3. Warwick Manufacturing Group (WMG), University of Warwick. Coventry, CV47AL, UK.

Abstract

A strategy for synthesis of nanostructured metal carbides that can convert oxides into carbides while maintaining their original nanomorphology is proposed in this study. TiC nanotube arrays (TiC NTAs) were successfully prepared by electrodeoxidation and carbonization in a low-temperature molten salt (600 ℃) using TiO_2 nanotube arrays (TiO_2 NTAs) as precursors. The effects of different factors on the heritability of nanostructures are discussed in detail. TiC NTAs have a highly ordered and directional array structure, a large specific surface area, excellent electrical conductivity, and outstanding chemical stability. Quasi-solid-state supercapacitor based on TiC NTA electrodes exhibit excellent electrochemical energy storage properties such as low charge transfer resistance, excellent cycle stability (90% retention after 10000 cycles), and high energy density (4.2 μWh cm^{-2}). This study demonstrates a high-performance supercapacitor nanoarray material and provides a general method for synthesis of nanostructured metal carbides.

KEYWORDS: ***TiC nanotube arrays, supercapacitors, nanomaterials, metal carbides, electrolysis***

1. INTRODUCTION

In order to mitigate the environmental problems caused by fossil energy, the development of clean and renewable energy (wind, solar, and tidal energy) has become an urgent concern. The supply of such energy sources is usually intermittent due to changes in the natural environment. Thus, highly efficient energy storage and conversion technologies are crucial for the utilization of renewable energy. Among the many energy storage devices, supercapacitors (SCs) have attracted great interest for their high power density, fast charge and discharge speed, long cycle life, safety, and environmental friendliness[1-3]. However, low energy density restricts their application and development. The performance of a SC mainly depends on the electrode material. An ideal electrode material should have a high specific surface area, regularity, and an adjustable nanostructure that increases the number of active sites for ion adsorption and redox reactions, increasing the SC capacity.

An ordered nanoarray is considered an ideal electrode structure to overcome the limitations of a traditional electrode structure[4-6]. The array structure can prevent accumulation of electrode materials, provide a greater surface area and smooth electron and ion transport paths, and increase the SC capacity and rate performance. The electrode material is usually grown directly on the current collector without additional adhesive or conductive additives, resulting in lower contact resistance and electrode self-weight. In recent decades, technologies for synthesizing nanostructure arrays have been reported, including atomic layer deposition (ALD)[7-9], electrochemical deposition [10,11], chemical vapor deposition[12], and reactive ion etching[13]. However, developing a simple, low-cost nanoarray fabrication process remains a challenge. With good electrical conductivity, high hardness, oxidation resistance, and corrosion resistance, TiC has recently attracted significant interest in the field of electrochemical energy storage and conversion[14-15]. A variety of nanostructured titanium carbides have demonstrated excellent SC performance[7, 16-18]. However, application of TiC array materials in energy storage electrode materials has seldom been reported. Current TiC

synthesis technology generally faces challenges such as high production temperature (> 1100 ℃) and difficult regulation of size and morphology[19-21].

In this study, a strategy is proposed to synthesize TiC nanotube arrays (TiC NTAs) materials and demonstrate their excellent SC performance. The process is based on TiO_2 nanotube arrays (TiO_2 NTAs) as the precursor, which are transformed into TiC NTAs in low-temperature molten salt. TiC NTAs have a high order and orientation and grow directly on the titanium current collector without additional binders. This remarkable structure provides a large specific surface area and a straight pathway for electron transport from the collector to the nanotube. However, maintaining perfect nanostructures during the transition from TiO_2 NTAs to TiC NTAs is a great challenge. Thus, the influence of different factors on nanostructure retention during the electrolysis process was studied. The TiC NTA electrode was assembled into a quasi-solid-state SC, exhibiting excellent electrochemical energy-storage performance.

2. Experiment

2.1 Preparation of TiO_2 NTAs

Titanium foil (thickness: 0.1 mm) or titanium mesh (100 mesh) was used as the anode and a platinum sheet was used as the counter electrode for anodization in an electrolyte of ethylene glycol-0.6 wt% NH_4F-2 vol% H_2O. First, the titanium foil was oxidized at 50 V for 1 h, and the TiO_2 NTAs on the surface were removed via ultrasonic treatment. After drying the titanium foil, oxidation was performed at 50 V for different times (15 min, 30 min and 1 h). Finally, the samples were annealed in the air at 400 ℃ for 1 h.

2.2 Preparation of TiC NTAs

TiC NTAs were manufactured in a sealed tubular electrolysis furnace. The LiCl–$CaCl_2$–KCl mixed molten salt (50:40:10 mol%) was added to a corundum crucible, dried at 300 ℃ for 12 h, and placed in an electrolytic furnace. The electrolytic furnace was sealed and vacuumed; then, high-purity argon was continuously introduced to maintain the inert atmosphere in the furnace. After the furnace was heated to the

specified temperature (500 ℃, 600 ℃, 700 ℃), with a stainless-steel rod as the cathode and a graphite rod as the anode, pre electrolysis was performed at 3 V for 12 h. Subsequently, different concentrations of Li_2CO_3 (0.05, 0.1, 1 mol%) were added to the molten salt as the carbon source, TiO_2 NTAs were added as the cathode precursor, and electrolysis was performed at 3.3 V for different periods of time. The obtained products were washed with dilute hydrochloric acid (0.5 mol/L) and deionized water and then dried under vacuum at 90 ℃.

2.3 Preparation of the Quasi-Solid-State SCs:

2 g of PVA was added to 20 mL deionized water and stirred at 80 ℃ for 1 h until completely dissolved. Then, 2 g of H_3PO_4 was slowly added and stirred for 2 h and finally dried at room temperature for 30 h to obtain an electrolyte thin film. A sandwich-type symmetrical flexible capacitor was assembled by using the titanium mesh, with TiC NTAs as electrodes and PVA−H_3PO_4 as the electrolyte and the separator.

2.4 Characterization

All samples were characterized by field-emission scanning electron microscopy (SEM, Thermo Fisher Scientific, Quattro S), x-ray diffraction (XRD, PANalytical X'PertPowder with Cu–Kα radiation, Panalytical B.V.), and transmission electron microscopy (TEM, Thermo Fisher Scientific, Talos F200S) and X-ray photoelectron spectroscopy (XPS, Thermo Fisher Scientific, ESCALAB 250Xi). In a threeelectrode system with 1 M Na_2SO_4 as the electrolyte, an Ag/AgCl electrode was used as the reference electrode, a platinum sheet was used as the counter electrode, and TiC NTAs was used as the working electrode. The electrochemical properties were tested on a CHI660E electrochemical workstation.

3. Results and discussion

3.1 Optimization of TiC NTAs Synthesis Parameters

The mechanism of converting TiO_2 nanotubes into TiC nanotubes is shown in **Figure 1a**. During the electrolysis process, TiO_2 is electro-deoxidized to form Ti. At

this time, CO_3^{2-} in the molten salt is reduced at the cathode to form carbon, which will react with Ti to form TiC. In addition to the CO_3^{2-} provided by the carbonate, the CO_2 bubbles formed on the anode will also be captured by the O^{2-} in the molten salt to form CO_3^{2-} [22-26], which together provide a carbon source for the carbonization of the metal Ti. However, It is a challenge for stable maintenance of the nanotube array structure during the transition from TiO_2 to TiC. Thus, the effects of electrolysis temperature, CO_3^{2-} concentration in the molten salt, anodization time, and electrolysis time on nanostructure retention were further studied.

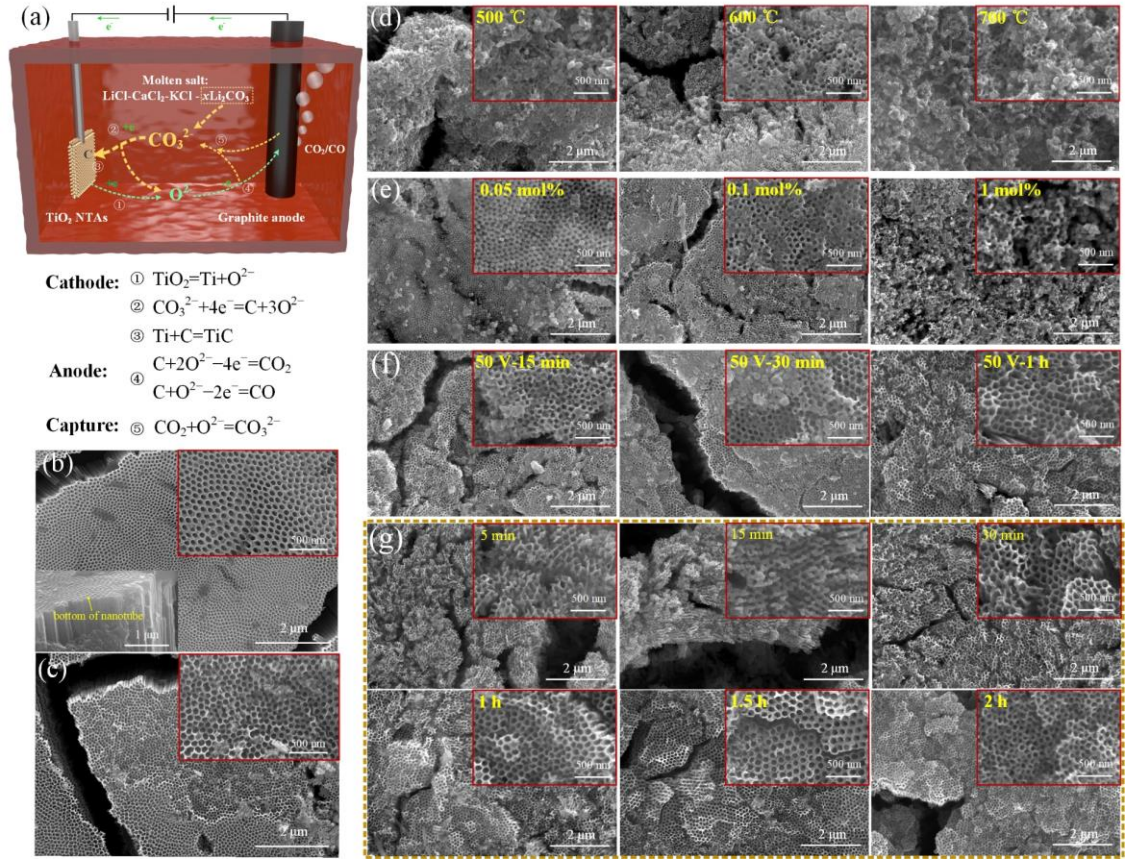

Figure 1. (a) Synthesis process of TiC NTAs; (b) TiO_2 NTAs formed after anodization at 50 V for 15 min (inset shows the bottom of the nanotube arrays); (c) TiO_2 NTAs after annealing; (d) SEM images of products at different electrolysis temperatures (500, 600, and 700 °C), while other parameters are constant (CO_3^{2-} concentration is 0.1 mol %, 50 V anodization for 15 min, and electrolysis time is 30 min); (e) SEM images of products with different CO_3^{2-} concentrations (0.05, 0.1, and 1 mol %), while other parameters are consistent (electrolysis temperatures is 600 °C, 50 V anodization for 15 min, and electrolysis time is 30 min); (f) SEM images of products with different anodizing times (15 min, 30 min, and 1 h), while other parameters are consistent (electrolysis temperatures is 600 °C, CO_3^{2-} concentration is 0.1 mol %, and electrolysis time is 30 min); (g) SEM

images of products with different electrolysis times (5 min, 15 min, 30 min, 1 h, 1.5 h, and 2 h), while other parameters are consistent (electrolysis temperatures is 600 °C, CO_3^{2-} concentration is 0.1 mol %, and 50 V anodization for 1 h).

TiO_2 NTAs are fabricated on titanium foil through the anodizing process (**Figure 1b**). The TiO_2 nanotubes are vertically arranged to form an array structure, each nanotube has a structure with bottom sealing and an upper opening, and the diameter is usually between 90 nm and 100 nm. **Figure 1c** shows an SEM image of TiO_2 NTAs after annealing at 400 ℃ for 1 h, and it can be seen that the morphology of the nanotubes is still intact. **Figure 1d** shows the morphology of the products after electrolysis at different temperatures. When the electrolysis temperature was 500 °C, almost no tubular morphology was observed in the product and the nanotubes was sintered together to form nano-nodular clusters, the main phase of the product is Ti_6O (**Figure S1)**. When the electrolysis temperature was increased to 600 ℃, some nanopores were observed in the product, and these nanopores can maintained a certain array structure. When the electrolysis temperature was 700 °C, nanopores and nanotubes had grown and coarsened to form nanostripes. Nanomaterials have a high surface free energy owing to their large specific surface area, so the sintering kinetics of nanomaterials are enhanced compared to conventional materials[27]. The sintering temperature is approximately 20–40% of the melting point temperature of the material[27]. The melting point of TiC (3140 °C) is much higher than that of Ti (1668 °C). when the electrolysis temperature was increased from 500 °C to 600 °C, severe sintering was avoided due to the formation of high-melting point TiC (**Figure S1)**. However, the TiC nanostructures gradually began to sinter and agglomerate with a further increase in electrolysis temperature. Thus, 600 °C is a more suitable electrolysis temperature, meeting the temperature requirements for TiC generation while preventing further sintering.

Figure 1e shows SEM images of the products after electrolysis in molten salts with different CO_3^{2-} concentrations. The relative diffraction peak intensity of TiC in the XRD pattern gradually increased with increasing CO_3^{2-} concentration (**Figure S2**), indicating that the carbonization reaction proceeded more fully. When the CO_3^{2-} concentration is 0.05 mol%, the product surface exhibits ordered TiC nanotubes, and the edge of the tube mouth becomes rounded due to sintering, and it also coalesced and coarsened of nanotube sidewalls in the lower part (**Figure S3)**. When the CO_3^{2-} concentration was 0.1 mol%, the sintering of the tube mouth and tube wall was

significantly less, and the nanotube wall diameter was almost the same as that of the tube mouth (**Figure S3)**. When the CO_3^{2-}concentration was increased to 1 mol%, and there were many damaged areas between the pores and the ordered nanopores almost completely disappeared. An appropriate CO_3^{2-} ion concentration in the molten salt is crucial for formation of TiC nanotubes. When the concentration was too low, the deposited carbon was insufficient to meet the needs of the carbonization reaction, and different degrees of sintering occurred at the tube mouth and sidewall. When the concentration was too high, with the charge competition between the CO_3^{2-} reduction reaction and deoxidation, titanium suboxides were present longer at high temperatures, resulting in nanotube collapse and degradation[28]. Thus, the appropriate CO_3^{2-} ion concentration in the molten salt is 0.1 mol%.

In the anodizing process, increasing the oxidation time promotes rearrangement and improves the order of TiO_2 nanotubes[29]. The improved order of nanotubes can prevent collapse and deformation caused by defect sites during electrolysis, which ensures the nanostructure stability and reduces cracking of the overall array structure. As shown in **Figure 1f**, with increased anodizing time, the nanotube diameter of the TiC products gradually increased, and the integrity of the nanostructures gradually improved. When TiO_2 NTAs were used as precursors after anodizing for 1 h, TiC products maintained the original nanotube array structure of TiO_2 NTAs, and the overall nanostructure was more complete than after anodizing for 15 min or 30 min.

The effect of electrolysis time on the retention of nanostructures during the conversion of TiO_2 NTAs to TiC NTAs was further studied (**Figure 1g)**. After electrolysis for 5 min and 15 min, TiC nanopores with rounded edges were observed in the products, the directions of the nanopores were relatively divergent. When the electrolysis time is more than 30min, the overall order of the TiC nanotube array was greatly improved, and the nanotube morphology is nearly undamaged after electrolysis for 1.5 h, the TiC NTAs completely maintain the nanomorphology of the TiO_2 NTAs precursor. The electrolysis time mainly affected the degree of sample carbonization (**Figure S4**). When electrolysis was performed for a short time, there were few TiC phases with high melting points in the product, and the uncarbonized part sintered

during slow cooling in the furnace, resulting in destruction of the nanostructure. With an increase in the electrolysis time, the degree of carbonization in the product gradually increased (**Figure S4)**, and the stability of the nanostructure at high temperatures gradually improved. When the electrolysis time is too long (electrolysis for 2 h), the Ti foil matrix is also carbonized, resulting in decreased toughness, which causes deformation of the TiC NTAs and brittle peeling of the coating (**Figure S5)**. Thus, 1.5 h was selected as the optimal electrolysis time.

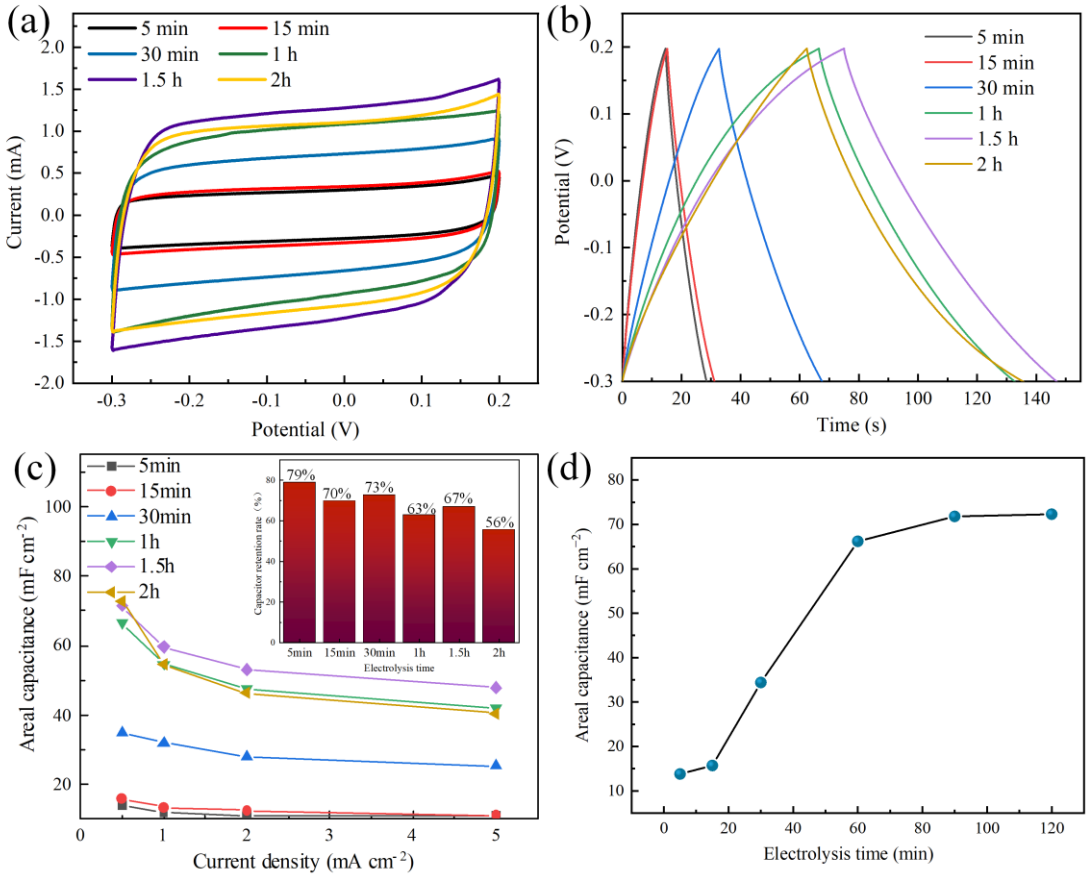

Figure 2. SC performance of TiC NTAs formed at different electrolysis times in 1 M Na_2SO_4 solution: (a) CV curves at 100 mv s^{-1}; (b) GCD curves with current density of 0.5 mA cm^{-2}; (c) area capacitance with different current densities. The inset shows the capacitance retention after the current density increases from 0.5 mA cm^{-2} to 5 mA cm^{-2}; (d) area specific capacitance of TiC NTAs formed at different electrolysis times with current density of 0.5 mA cm^{-2}.

The specific capacitance of TiC NTAs is closely related to their integrity and degree of carbonization. For highly oriented and ordered nanotube arrays, the electrode material can provide a larger surface area to form an electric double layer, so a higher

areal specific capacitance can be achieved. Moreover, **Figure S6** shows that the TiC flake can produce a higher area capacitance (0.53 mF cm^{-2} at a current density of 0.05 mA cm^{-2}) than Ti flake (0.06 mF cm^{-2} at a current density of 0.01 mA cm^{-2}), so the electrode material with a higher degree of carbonization has a higher capacitance. **Figure 2** shows the variation trend of the area specific capacitance of TiC NTAs with electrolysis time. When the electrolysis time was less than 1 h, the nanostructure integrity of the TiC NTAs gradually improved, the degree of carbonization gradually increased (**Figure S4**), and the area specific capacitance increased rapidly. When the electrolysis time was greater than 1 h, the morphology and carbonization degree of the TiC NTAs exhibited little difference, and the area specific capacitance gradually stabilized. The TiC NTA material formed by electrolysis for 1.5 h had an ordered tubular array structure and excellent electrochemical energy-storage performance.

3.2 Fabrication of TiC NTAs on Titanium Mesh

The porous electrode structure with higher specific surface area was further constructed using titanium mesh as the matrix（**Figure 3a**）. As shown in **Figure 3b-d**, uniform titanium dioxide nanotubes are formed on the surface of the titanium mesh after anodic oxidation at 50 V for 1 h. The nanotubes diverge at different angles based on the radian of the titanium wire surface. According to the research in Section 3.1, the TiO_2 NTAs were electrolyzed at 600 ℃ for 1.5 h with 0.1 mol% CO_3^{2-} in molten salt. The morphology and length of the TiC NTAs were basically consistent with the TiO_2 NTAs precursor（**Figure 3e-g**）.

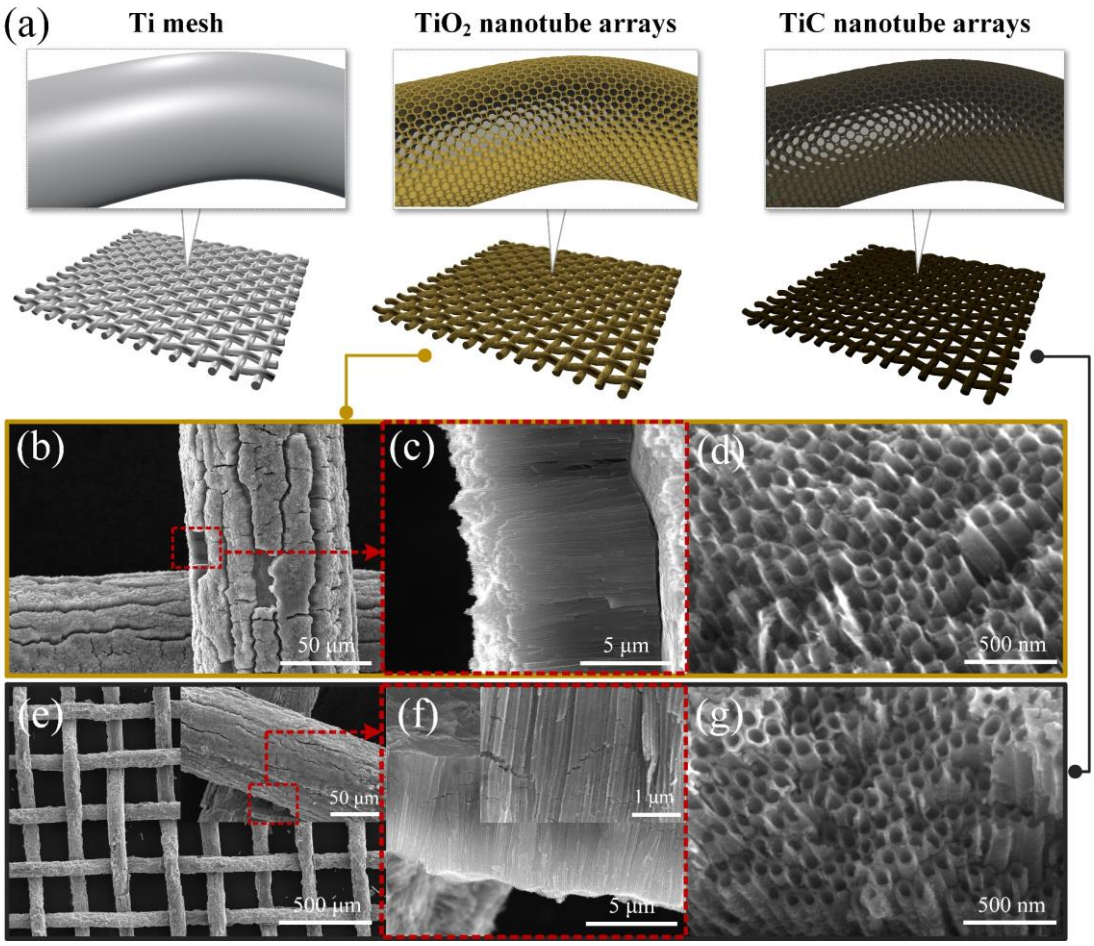

Figure 3. (a) Schematic of the fabrication process of TiC NTAs on titanium mesh; (b) − (d) SEM images of TiO_2 NTAs: (b) low-magnification view of the TiO_2 NTAs on titanium mesh; (c) side view of TiO_2 NTAs; (d) top view of TiO_2 NTAs; (e) − (g) SEM images of TiC NTAs: (b) low-magnification view of the TiC NTAs on titanium mesh; (c) side view of TiC NTAs; (d) top view of TiC NTAs.

The microscopic morphology of the samples after electrolysis for 1.5 h was analyzed by TEM. A hollow tubular morphology is clearly observed in **Figure 4a**, and elemental mapping analysis of Ti and C further confirmed the nanotube composition (**Figure 4b**). In addition, the SAED diagram shows typical TiC crystalline ring characteristics, and the adjacent lattice spacing is 0.22 nm (**Figure 4c**), corresponding to the (200) crystal plane of cubic TiC (JCPDS 65-0242). The characteristic peaks of the electrolytic products are mainly TiC and the titanium matrix in the XRD pattern (**Figure 4d**). In addition, the surface elemental composition of the TiC NTAs was analyzed by XPS (**Figure 4e**). For the Ti 2p spectrum, two obvious peaks at Ti $2p_{1/2}$

(460.5 eV) and Ti $2p_{3/2}$ (454.8 eV) were observed, which correspond to the Ti−C bond[30]. In the C 1s spectra, the peak at 281.7 eV is attributed to carbon atoms in TiC[31].

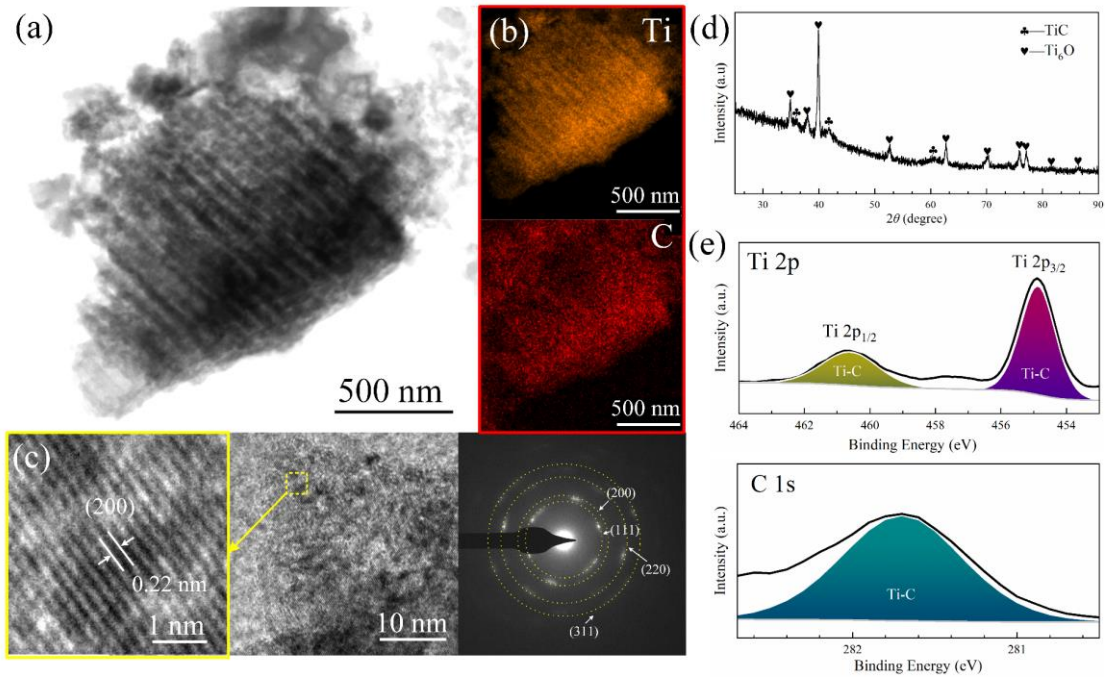

Figure 4. (a) TEM images of TiC NTAs; (b) elemental mapping of Ti and C; (c) corresponding SAED pattern and HRTEM image; (e) XRD pattern of TiC NTAs; (d) XPS spectra of TiC NTAs.

3.6 SC Performance

To evaluate the application potential of TiC NTAs materials in SC, we assembled a quasi-solid-state SC was assembled with PVA-H_3PO_4 as the electrolyte and TiC NTAs as the electrode (**Figure 5a**). **Figure 5b** shows that the CV curve maintains a quasi-rectangular shape at scanning speeds of 10–100 mV s^{-1}. Typical linear charge–discharge curves were observed in the GCD (**Figure 5c)**, further demonstrating the EDLC behavior and good reversibility of the TiC NTAs electrode. **Figure 5d** shows the specific capacitance of the TiC NTAs electrode with different current densities. The area specific capacitance reaches 83 mF cm^{-2} at a current density of 0.5 mA cm^{-2}， and the energy density reaches 4.2 μWh cm^{-2} at a power density of 149.4 μWh cm^{-2} (**Figure 5f**), higher than values reported for other quasi-solid-state SCs[32-37].

Figure 5e shows the Nyquist plots of the SC. Fitting the Nyquist plot indicates an internal resistance (R_s) of 1.17 Ω and a charge transfer resistance (R_{ct}) of 0.48 Ω, the

lower resistance is attributed to the unique nanostructure of TiC NTAs. The TiC nanotube adheres to the Ti substrate, and electrons can be directly transferred from the Ti collector to all parts of the tube array. Thus, it exhibits excellent conductivity, and the electrode does not require additional conductive adhesive, further reducing the internal resistance. The highly oriented, hollow tubular structure of TiC NTAs provides more electrode/electrolyte interfaces, increases the electron transfer pathways, and provides a smooth channel for ion transmission, greatly reducing the charge transfer resistance at the interface. The cyclic life of the flexible device at a current density of 5 mA cm^{-2} was also tested (**Figure 5g)**. The capacitance of the flexible device gradually increased in the first 1000 cycles due to the self-activation process. [38,39] The flexible device maintained 90% of its initial capacity after 10,000 cycles.

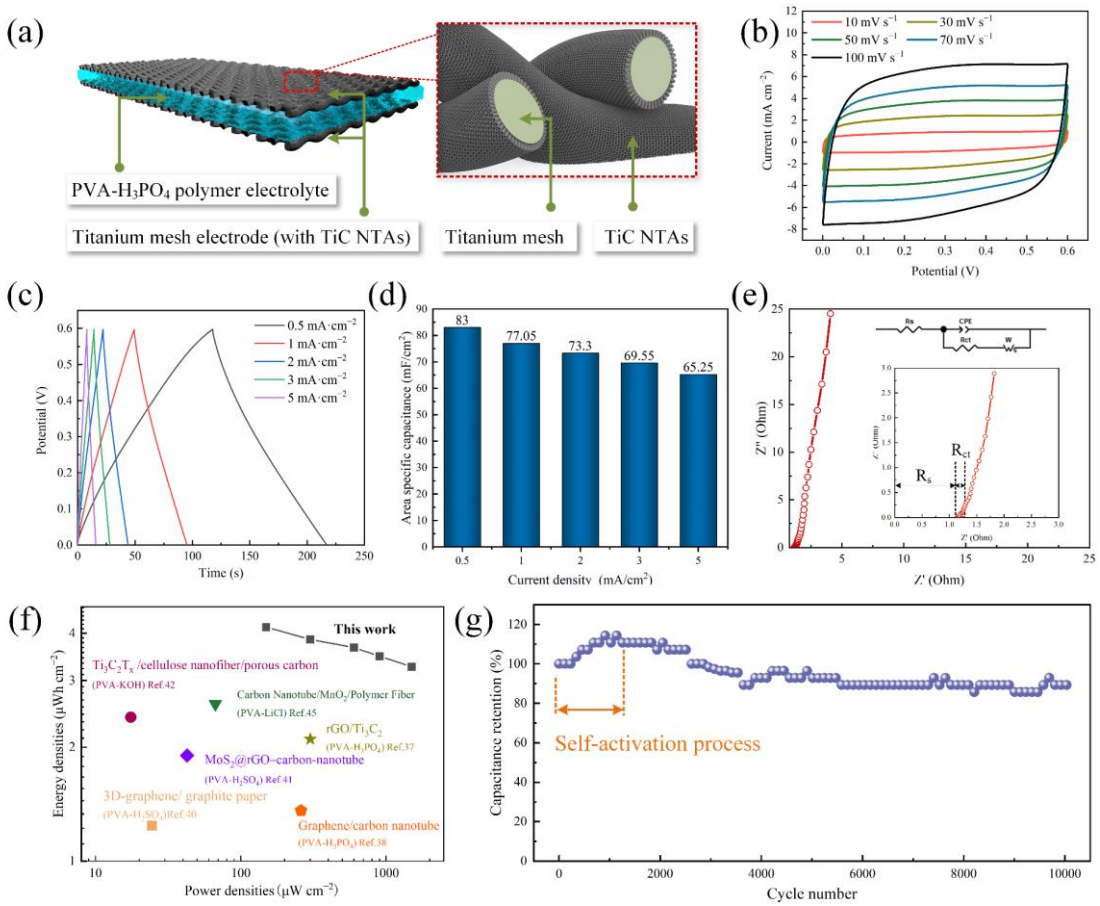

Figure 5. SC performance of TiC NTAs in PVA-H_3PO_4. (a) Schematic of a quasi-solid SC; (b) CV curves at different scan rates; (c) GCD curves at different current densities; (d) specific capacitances at different current densities; (e) Nyquist plots (high-frequency range details and the equivalent

circuit in inset); (f) ragone plot of TiC NTAs and other quasi-solid flexible SCs; (g) cycling performance of TiC NTAs.

4. CONCLUSIONS

In this study, a strategy for synthesis of nanostructured metal carbides is proposed, using nanostructured metal oxides as precursors to form corresponding nanostructured metal carbides after deoxidation and carbonization in a low-temperature molten salt (600 ℃). This technology has the advantages of simplicity, low cost, and a far lower temperature than traditional TiC synthesis. TiO_2 NTAs were successfully transformed into TiC NTAs. The effects of different factors on the heritability of nanostructures during the oxide-to-carbide process were discussed in detail. For electrochemical energy storage, TiC NTAs have a large specific surface area, good electrical conductivity, a highly ordered and directional array structure, and exhibit excellent SC performance. This study demonstrates a high-performance SC nanoarray material and provides a general method for the synthesis of nanostructured metal carbides.

Supporting Information

XRD pattern of product after electrolysis at different temperatures (**Fig. S1)**; XRD pattern of product with different CO_3^{2-} concentrations (**Fig. S2)**; SEM images of TiC nanotube sidewalls with different CO_3^{2-} concentrations (**Fig. S3)**; XRD pattern of product with different electrolysis times (**Fig. S4)**; SEM images and photo of TiC nanotube arrays after electrolysis for 2 h (**Fig. S5)**.

Acknowledgements

Funding: This work was supported financially support by the National Natural Science Foundation of China (No. 52174299), and supported by the Chongqing Key Laboratory of Vanadium-Titanium Metallurgy and New Materials, Chongqing University, Chongqing 400044, PR China.

References

(1) González, A.; Goikolea, E.; Barrena, J. A.; Mysyk, R., Review on supercapacitors: Technologies and materials. *Renewable Sustainable Energy Rev.* **2016,** *58*, 1189-1206.

(2) Yu, Q.; Lv, J.; Liu, Z.; Xu, M.; Yang, W.; Owusu, K. A.; Mai, L.; Zhao, D.; Zhou, L. Macroscopic Synthesis of Ultrafine N-doped Carbon Nanofibers for Superior Capacitive Energy Storage. Sci. Bull. 2019, 64, 1617−1624.

(3) Owusu, K. A.; Wang, Z. Y.; Qu, L.; Liu, Z. A.; Mehrez, J. A. A.; Wei, Q. L.; Zhou, L.; Mai, L. Q. Activated Carbon Clothes for Widevoltage High-energy-density Aqueous Symmetric Supercapacitors. Chin. Chem. Lett. 2020, 31, 1620−16243.Zhao, H.;

(4) Zhou, M.; Wen, L.; Lei, Y., Template-directed construction of nanostructure arrays for highly-efficient energy storage and conversion. *Nano Energy* **2015,** *13*, 790-813.

(5) Wang, Z.; Cao, D.; Xu, R.; Qu, S.; Wang, Z.; Lei, Y., Realizing ordered arrays of nanostructures: A versatile platform for converting and storing energy efficiently. *Nano Energy* **2016,** *19*, 328-362.

(6) Lu, X.; Zheng, D.; Zhai, T.; Liu, Z.; Huang, Y.; Xie, S.; Tong, Y., Facile synthesis of large-area manganese oxide nanorod arrays as a high-performance electrochemical supercapacitor. *Energy and Environmental Science* **2011,** *4* (8), 2915-2921.

(7) Zhong, Y.; Xia, X.; Zhan, J.; Wang, Y.; Wang, X.; Tu, J., Monolayer titanium carbide hollow sphere arrays formed via an atomic layer deposition assisted method and their excellent high-temperature supercapacitor performance. *Journal of Materials Chemistry A* **2016,** *4* (48), 18717-18722.

(8) Wang, R.; Xia, C.; Wei, N.; Alshareef, H. N., $NiCo_2O_4$@TiN core-shell electrodes through conformal atomic layer deposition for all-solid-state supercapacitors. *Electrochim. Acta* **2016,** *196*, 611-621.

(9) Wen, L.; Zhou, M.; Wang, C.; Mi, Y.; Lei, Y., Nanoengineering energy conversion and storage devices via atomic layer deposition. *Advanced Energy Materials* **2016,** *6* (23), 1600468.

(10) Chen, W.; Xia, C.; Alshareef, H. N., One-step electrodeposited nickel cobalt sulfide nanosheet arrays for high-performance asymmetric supercapacitors. *ACS Nano* **2014,** *8* (9), 9531-9541.

(11) Xia, X.; Chao, D.; Qi, X.; Xiong, Q.; Zhang, Y.; Tu, J.; Zhang, H.; Fan, H. J., Controllable growth of conducting polymers shell for constructing high-quality organic/inorganic core/shell nanostructures and their optical-electrochemical properties. *Nano Lett.* **2013,** *13* (9), 4562-4568.

(12) Malik, R.; Zhang, L.; McConnell, C.; Schott, M.; Hsieh, Y. Y.; Noga, R.; Alvarez, N. T.; Shanov, V., Three-dimensional, free-standing polyaniline/carbon nanotube composite-based electrode for high-performance supercapacitors. *Carbon* **2017,** *116*, 579-590.

(13) Maeng, J.; Kim, Y. J.; Meng, C.; Irazoqui, P. P., Three-dimensional microcavity array electrodes for high-capacitance all-solid-state flexible microsupercapacitors. *ACS Applied Materials and Interfaces* **2016,** *8* (21), 13458-13465.

(14) Chen, T.; Li, M.; Song, S.; Kim, P.; Bae, J., Biotemplate preparation of multilayered TiC nanoflakes for high performance symmetric supercapacitor. *Nano Energy* **2020,** *71*, 104549.

(15) Dong, B. X.; Qiu, F.; Li, Q.; Shu, S. L.; Yang, H. Y.; Jiang, Q. C., The synthesis, structure, morphology characterizations and evolution mechanisms of nanosized titanium carbides and their further applications. *Nanomaterials* **2019,** *9* (8), 1152.

(16) Xia, X.; Zhang, Y.; Chao, D.; Xiong, Q.; Fan, Z.; Tong, X.; Tu, J.; Zhang, H.; Fan, H. J., Tubular TiC fibre nanostructures as supercapacitor electrode materials with stable cycling life and wide-temperature performance. *Energy and Environmental Science* **2015,** *8* (5), 1559-1568.

(17) Xia, X.; Zhan, J.; Zhong, Y.; Wang, X.; Tu, J.; Fan, H. J., Single-crystalline, metallic TiC nanowires for highly robust and wide-temperature electrochemical energy storage. *Small* **2017,** *13* (5), 1602742.
(18) Krishnamoorthy, K.; Pazhamalai, P.; Sahoo, S.; Kim, S. J., Titanium carbide sheet based high performance wire type solid state supercapacitors. *Journal of Materials Chemistry A* **2017,** *5* (12), 5726-5736.
(19) Zhong, J.; Liang, S.; Zhao, J.; Wu, W. D.; Liu, W.; Wang, H.; Chen, X. D.; Cheng, Y. B., Formation of novel mesoporous TiC microspheres through a sol-gel and carbothermal reduction process. *J. Eur. Ceram. Soc.* **2012,** *32* (12), 3407-3414.
(20) Taguchi, T.; Yamamoto, H.; Shamoto, S. I., Synthesis and characterization of single-phase TiC nanotubes, TiC nanowires, and carbon nanotubes equipped with TiC nanoparticles. *J. Phys. Chem. C* **2007,** *111* (51), 18888-18891.
(21) Tao, X.; Du, J.; Yang, Y.; Li, Y.; Xia, Y.; Gan, Y.; Huang, H.; Zhang, W.; Li, X., TiC nanorods derived from cotton fibers: Chloride-assisted VLS growth, structure, and mechanical properties. *Cryst. Growth Des.* **2011,** *11* (10), 4422-4426.
(22) Chen, G. Z., Interactions of molten salts with cathode products in the FFC Cambridge Process. *International Journal of Minerals, Metallurgy and Materials* **2020,** *27* (12), 1572-1587.
(23) Chen, G. Z.; Fray, D. J., Invention and fundamentals of the FFC Cambridge Process. In *Extractive Metallurgy of Titanium: Conventional and Recent Advances in Extraction and Production of Titanium Metal*, 2019; pp 227-286.
(24) Yuan, Y.; Li, W.; Chen, H.; Wang, Z.; Jin, X.; Chen, G. Z., Electrolysis of metal oxides in MgCl2 based molten salts with an inert graphite anode. *Faraday Discuss.* **2016,** *190*, 85-96.
(25) Weng, W.; Wang, M.; Gong, X.; Wang, Z.; Wang, D.; Guo, Z., Mechanism analysis of carbon contamination and the inhibition by an anode structure during soluble K_2CrO_4 electrolysis in $CaCl_2$-KCl molten salt. *J. Electrochem. Soc.* **2017,** *164* (12), E360-E366.
(26) Chen, X.; Zhao, H.; Xie, H.; Qu, J.; Ding, X.; Geng, Y.; Wang, D.; Yin, H., Tuning the preferentially electrochemical growth of carbon at the "gaseous CO_2-liquid molten salt-solid electrode" three-phase interline. *Electrochim. Acta* **2019,** *324*, 134852.
(27) Ramos, J. P.; Senos, A. M. R.; Stora, T.; Fernandes, C. M.; Bowen, P., Development of a processing route for carbon allotrope-based TiC porous nanocomposites. *J. Eur. Ceram. Soc.* **2017,** *37* (13), 3899-3908.
(28) Shivaram, A.; Bose, S.; Bandyopadhyay, A., Thermal degradation of TiO_2 nanotubes on titanium. *Appl. Surf. Sci.* **2014,** *317*, 573-580.
(29) Regonini, D.; Bowen, C. R.; Jaroenworaluck, A.; Stevens, R., A review of growth mechanism, structure and crystallinity of anodized TiO_2 nanotubes. *Materials Science and Engineering R: Reports* **2013,** *74* (12), 377-406.
(30) Cheng, Y.; Zheng, Y. F., Characterization of TiN, TiC and TiCN coatings on Ti-50.6 at.% Ni alloy deposited by PIII and deposition technique. *Surf. Coat. Technol.* **2007,** *201* (9-11 SPEC. ISS.), 4909-4912.
(31) Lewin, E.; Persson, P. O. Å.; Lattemann, M.; Stüber, M.; Gorgoi, M.; Sandell, A.; Ziebert, C.; Schäfers, F.; Braun, W.; Halbritter, J.; Ulrich, S.; Eberhardt, W.; Hultman, L.; Siegbahn, H.; Svensson, S.; Jansson, U., On the origin of a third spectral component of C1s XPS-spectra for nc-TiC/a-C nanocomposite thin films. *Surf. Coat. Technol.* **2008,** *202* (15), 3563-3570.
(32) Ramadoss, A.; Yoon, K. Y.; Kwak, M. J.; Kim, S. I.; Ryu, S. T.; Jang, J. H., Fully flexible, lightweight, high performance all-solid-state supercapacitor based on 3-Dimensional-graphene/graphite-paper. *J.*

Power Sources **2017,** *337*, 159-165.
(33) Choi, C.; Kim, S. H.; Sim, H. J.; Lee, J. A.; Choi, A. Y.; Kim, Y. T.; Lepró, X.; Spinks, G. M.; Baughman, R. H.; Kim, S. J., Stretchable, weavable coiled carbon nanotube/MnO_2/polymer fiber solid-state supercapacitors. *Scientific Reports* **2015,** *5*, 59387.
(34) Yang, W.; He, L.; Tian, X.; Yan, M.; Yuan, H.; Liao, X.; Meng, J.; Hao, Z.; Mai, L., Carbon-MEMS-based alternating stacked MoS_2@rGO-CNT micro-supercapacitor with high capacitance and energy density. *Small* **2017,** *13* (26), 17000639.
(35) Chen, W.; Zhang, D.; Yang, K.; Luo, M.; Yang, P.; Zhou, X., Mxene ($Ti_3C_2T_x$)/cellulose nanofiber/porous carbon film as free-standing electrode for ultrathin and flexible supercapacitors. *Chem. Eng. J.* **2021,** *413*, 127524.
(36) Radha, N.; Kanakaraj, A.; Manohar, H. M.; Nidhi, M. R.; Mondal, D.; Nataraj, S. K.; Ghosh, D., Binder free self-standing high performance supercapacitive electrode based on graphene/titanium carbide composite aerogel. *Appl. Surf. Sci.* **2019,** *481*, 892-899.
(37) Wang, Y. L.; Zhang, Y.; Wang, G. L.; Shi, X. W.; Qiao, Y. D.; Liu, J. M.; Liu, H. G.; Ganesh, A.; Li, L. Direct Graphene-Carbon Nanotube Composite Ink Writing All-Solid-State Flexible Microsupercapacitors with High Areal Energy Density. *Adv. Funct. Mater.* **2020,** *30* (16), 1907284.
(38) Lu, X.; Wang, G.; Zhai, T.; Yu, M.; Xie, S.; Ling, Y.; Liang, C.; Tong, Y.; Li, Y., Stabilized TiN nanowire arrays for high-performance and flexible supercapacitors. *Nano Lett.* **2012,** *12* (10), 5376-5381.
(39) Li, H.; Liu, Y.; Lin, S.; Li, H.; Wu, Z.; Zhu, L.; Li, C.; Wang, X.; Zhu, X.; Sun, Y., Laser crystallized sandwich-like MXene/Fe_3O_4/MXene thin film electrodes for flexible supercapacitors. *J. Power Sources* **2021,** *497*, 229882.